



# Abrupt monsoonal shifts over the precessional cycles documented in Yongxing Cave in China during the antepenultimate glacial period

Yijia Liang<sup>1,2,3</sup> · Shitao Chen<sup>1,2,3</sup> · Zhenqiu Zhang<sup>4</sup> · Shaohua Yang<sup>1,2,3</sup> · Mingxia Li<sup>1,2,3</sup> · Hai Cheng<sup>5</sup> · Yongjin Wang<sup>1,2,3</sup>

Received: 14 January 2017 / Accepted: 9 March 2018 / Published online: 15 March 2018  
© Springer-Verlag GmbH Germany, part of Springer Nature 2018

## Abstract

Precession is the major orbital control of monsoon intensity, but the monsoonal response to the transition between precessional cycles has yet to be explored. Here, we present an Asian Summer Monsoon history that spans 327.7–280.5 ka BP based on a <sup>230</sup>Th-dated and centennially resolved multi-proxy speleothem record from Yongxing Cave, central China. The  $\delta^{18}\text{O}$  profile, a proxy of monsoon intensity, follows the summer insolation changes, with three abrupt shifts occurring at precessional transitions. These shifts are supported by the stalagmite  $\delta^{13}\text{C}$ , grey-level and petrography analysis, indicating a coherent link between the karst processes and monsoon changes. Evidence from the coeval rapid changes in atmospheric  $\text{CH}_4$  and forest evolution records within dating errors suggests a wider regional signal of monsoon changes. The weak monsoon intervals are temporally consistent with the ice-rafted debris layers in the North Atlantic, indicating a strong coupling of the high- and low-latitude climate systems. We speculate that the abrupt monsoonal shifts are initiated by the south–north shifts of the Intertropical Convergence Zone associated with the Atlantic Meridional Overturning Circulation and further amplified by land cover. In addition, the rates and magnitudes of insolation changes modify monsoon shifts, thus indicating the abrupt monsoonal shift as a result of an interaction of orbital and millennial forcing.

**Keywords** Chinese stalagmite · Asian Monsoon · Abrupt shifts · Precession cycle · Interaction

## Introduction

Earth's stochastic climate is modulated by cyclic variations in the orbital parameters, and it is well established from records that the 23-ka precession cycle of the Earth's rotational axis alters the global monsoonal system (deMenocal et al. 2000; Wang et al. 2008; Ziegler et al. 2010; Cheng et al. 2016). In

theory, monsoon should respond directly and synchronously to precession-induced insolation changes (Kutzbach 1981). However, records from Chinese caves have shown that most of the Asian Monsoon (AM) Termination I occurred within 200 years (Wang et al. 2001) and that most of the AM Termination II occurred within 70 years (Kelly et al. 2006), faster than the changing rate of solar insolation. The rapid termination that characterized the last two glacial periods pertained to the third-, fourth-, fifth-, sixth-most recent glacial–interglacial transitions (Cheng et al. 2009, 2016). These abrupt monsoonal jumps with respect to the gradual insolation rise also occurred in the Holocene (deMenocal et al. 2000) and the MIS (Marine Isotope Stage) 4/3 and MIS 5.2/5.1 boundaries (Liu et al. 2010; Schaefer et al. 2015; Cheng et al. 2016), indicating a self-similarity of the climate system. The involvement of a ‘tipping point’ has been proposed to be the primary control of the abrupt shifts (Yuan et al. 2004; Kelly et al. 2006). And strongly nonlinear self-amplifying feedbacks such as vegetation are suggested to force the abrupt climate change (deMenocal et al. 2000; Levermann et al. 2009). Other studies propose the link between AM and abrupt North Atlantic climate fluctuations (Wang et al. 2001, 2008; Yuan et al. 2004)

✉ Shitao Chen  
09100@njnu.edu.cn

<sup>1</sup> College of Geography Science, Nanjing Normal University, Nanjing 210023, China

<sup>2</sup> State Key Laboratory Cultivation Base of Geographical Environment Evolution (Jiangsu Province), Nanjing 210023, China

<sup>3</sup> Jiangsu Center for Collaborative Innovation in Geographical Information Resource Development and Application, Nanjing 210023, China

<sup>4</sup> School of History Geography and Tourism, Shangrao Normal University, Shangrao 334001, China

<sup>5</sup> Institute of Global Environmental Change, Xi'an Jiaotong University, Xi'an 710049, China

due to the fact that changes of Atlantic Meridional Overturning Circulation (AMOC) perturb atmospheric circulation and influence the displacement of the Intertropical Convergence Zone (ITCZ) (Chiang et al. 2014).

Several authors have attempted to determine the relationship between millennial and orbital changes and their impacts on climate. For example, it is proposed that both rising insolation and disintegrated ice sheets generated positive feedbacks driving the terminations (Cheng et al. 2009). Wang et al. (2008) suggested that the superposition of millennial-scale events resulted in a lag of the AM relative to insolation during the Heinrich 11 (H11) episode. The absence of millennial warming events in the northern hemisphere could have caused the glacial terminations (Wolff et al. 2009), and millennial changes in the zonality of atmospheric circulation over the North Atlantic were linked to precession via sea ice feedbacks (Siddall et al. 2010). The monsoonal system has demonstrated itself to be complicated (Mohtadi et al. 2016), but fortunately the absolutely dated Chinese stalagmites provide an insight into the monsoon evolution which will provide a target for detecting the interaction between orbital and millennial variability.

MIS 9, a period of small- to intermediate-sized ice volume, is the third-most recent interglacial period characterized by high concentration of greenhouse gases, large amplitude of temperature changes and abrupt climate and vegetation changes (Petit et al. 1999; McManus et al. 1999; Loulergue et al. 2008; Barker et al. 2011; Fletcher et al. 2013). The longest AM record covers the past 641 ka BP (Cheng et al. 2016), but the resolution during MIS 9 is only ~480 years relative to the entire 77-year resolved record and hence insufficient to study millennial-scale monsoon variability. Detailed millennial- and orbital-scale changes of AM, however, were discussed over the last two glacial cycles (Wang et al. 2008). Besides, the long-term monsoon changes are dominantly recorded in  $\delta^{18}\text{O}$  records (Cheng et al. 2016), and they lack support from proxies such as the  $\delta^{13}\text{C}$  and grey level. Here, we present a high-resolution and multi-proxy stalagmite record from Yongxing Cave, central China, spanning the interval between 327.7 and 280.5 ka BP. Our record refines the low-resolution record from Linzhu Cave (Cheng et al. 2009, 2016) and allows a detailed assessment of millennial-scale AM changes during MIS 9. Based on evidence suggesting a close link to orbital forcing and a quick response to high-latitude climate, we discuss the characteristics and mechanisms of abrupt shifts over precession cycles of this period.

## Materials and methods

### Site and sample description

Yongxing Cave (31°35'N, 111°14'E) is located at an elevation of 750 m on the east slope of Mt. Shennongjia

(Fig. 1). The cave atmosphere is isolated from the ambient atmosphere due to its narrow entrance, and the relative humidity inside is ~100%. The mean annual surface air temperature is ~12 °C, and the mean annual rainfall is ~1000 mm. During the boreal summer (June to September), the inland flow of warm and humid air from the tropical Indo-Pacific delivers approximately 80% of the total annual precipitation.

A candle-shaped stalagmite (sample YX15) was collected from the western floor of the second chamber in Yongxing Cave. It has a total length of 678 mm, and was cut and polished along its growth axis. Growth interruptions are present between 400 and 0 mm from the top. In this study, we use the lower part (678–400 mm from the top), whose stratigraphy is clear and the apex shape is convex upward, indicating stable growth at a regular drip rate.

Between 678 and 400 mm from the top, a remarkable alternation of beige-porous and dark compact calcite is observed. The colourless calcite occurs essentially between 600 and 542 mm and between 475 and 400 mm, and the remainder is predominantly comprised of darker calcite. According to the petrographic feature, the profile is divided into four parts (Fig. 2d). The dark compact segments are transparent, and their laminae are less visible and inter-layered with light-coloured bandings. The beige-porous segments are translucent, with white and fibrous crystals elongated parallel to the growth direction. The transitions between different coloured parts and the petrographic changes are clearly identified by grey-level profile (Fig. 2c).

### Analytical methods

Nine subsamples (~100–150 mg) were collected with 0.9-mm-diameter hand-held carbide dental burrs for  $^{230}\text{Th}$  dating. Five dates were analysed on a Finnigan Element inductively coupled plasma mass spectrometer (ICP-MS) at the Department of Geology and Geophysics, University of Minnesota, USA. The other dates were obtained using a multi-collector inductively coupled plasma mass spectrometer (MC-ICP-MS) at the Institute of Global Environmental Change, Xi'an Jiaotong University, China. The chemical procedures were similar to those described in Cheng et al. (2013), and the results are listed in Table 1.

A total of 279 subsamples (~50–100  $\mu\text{g}$ ) were drilled for oxygen and carbon isotopic measurements along the growth axis at a spacing of 1 mm with 0.3-mm-diameter carbide dental burrs. The analyses were conducted using a Finnigan MAT 253 mass spectrometer linked to a Kiel Carbonate Device at the College of Geography Science, Nanjing Normal University. The results are reported in parts per mil relative to Vienna Pee Dee Belemnite (VPDB) and with standardization accomplished using

**Fig. 1** Geographical overview of Chinese caves, including the sites of Yongxing (31°35'N, 111°14'E), Hulu (32°30'N, 119°10'E), Sanbao (31°40'N, 110°26'E), Linzhu (31°31'N, 111°19'E) and Dongge (25°17'N, 108°5'E) caves. The arrows depict the wind direction of the Asian Summer Monsoon and the Indian Summer Monsoon

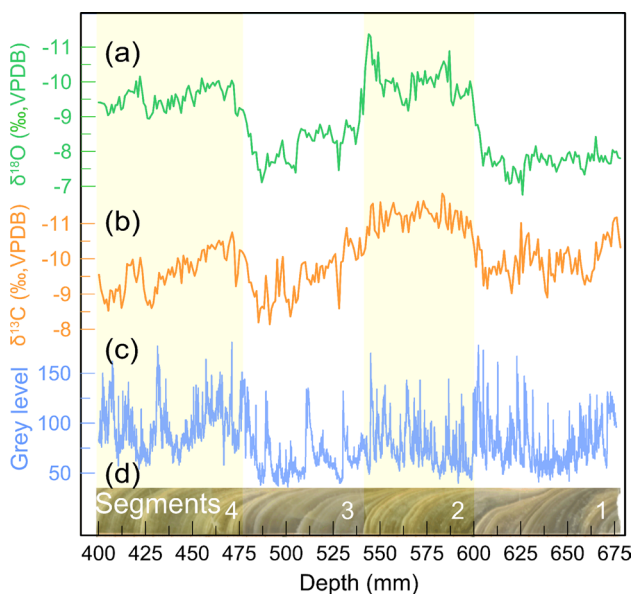
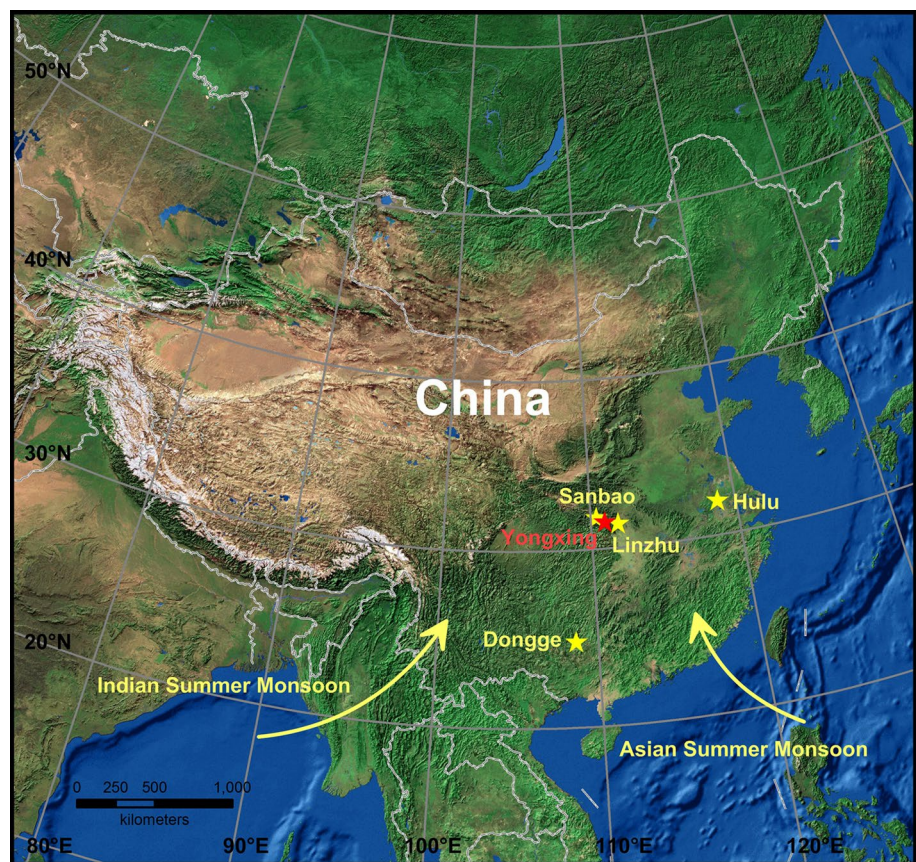


**Fig. 2** Multiple proxies of the YX15 stalagmite. **a**  $\delta^{18}\text{O}$ , **b**  $\delta^{13}\text{C}$  and **c** grey-level records and **d** cut face. The coloured bars indicate the four petrographic segments

NBS19. The precision is 0.06‰ for  $\delta^{18}\text{O}$  and 0.05‰ for  $\delta^{13}\text{C}$  at the 1 $\sigma$  level.

For the grey-level measurements, the polished surface of the studied section was scanned at a resolution of 1200 dpi using an EPSON Perfection 4990 Photo Scanner. The grey level was then obtained from the image using the Environment for Visualizing Images (ENVI 4.7) software while traversing down the growth axis. The values range between 36 and 181, with a spatial resolution of 20  $\mu\text{m}$ .

## Results

### Chronology

Nine dates for sample YX15 are given in Table 1 and indicate a period of deposition from  $322.6 \pm 8.1$  to  $279.0 \pm 2.1$  ka BP, equivalent to MIS 9. The  $^{238}\text{U}$  concentration ranges from 508 to 746 ppb, and the  $^{232}\text{Th}$  concentration ranges from 422 to 3943 ppt. The average 2 $\sigma$  error of the corrected  $^{230}\text{Th}$  ages is 1.4%, with a maximum of 2.5% (YX15-629) and a minimum of 0.7% (YX15-402). The dates are in stratigraphic order, with two exceptions (YX15-500 and YX15-668).

It is likely that short-lived growth cessations exist, but the thousand-year dating errors cannot resolve small hiatuses.

**Table 1**  $^{230}\text{Th}$  dating results for YX15 stalagmite

Sample number	Depth (mm)	$^{238}\text{U}$ (ppb)	$^{232}\text{Th}$ (ppt)	$\delta^{234}\text{U}$ (measured)	$[\text{}^{230}\text{Th}/\text{}^{238}\text{U}]$ (activity)	$^{230}\text{Th}$ age (ka BP) (uncorrected)	$^{230}\text{Th}$ age (ka BP) (corrected)
YX15-402*	402	526.1	3327.2	558.6	1.6	279.1 ± 2.1	279.0 ± 2.1
YX15-480	480	683.3	1160.5	527.9	1.6	290.9 ± 4.0	290.9 ± 4.0
YX15-490	490	746.6	1024.4	513.6	1.6	294.5 ± 5.6	294.4 ± 5.6
YX15-500*	500	593.7	1420.8	510.8	1.6	293.9 ± 2.2	293.8 ± 2.2
YX15-541*	541	596.6	704.8	506.6	1.6	302.1 ± 2.6	302.0 ± 2.6
YX15-597*	597	508.7	422.3	365.9	1.4	311.7 ± 3.6	311.6 ± 3.6
YX15-604	604	567.1	3943.1	427.2	1.5	313.4 ± 6.3	313.3 ± 6.3
YX15-629	629	562.5	634.9	456.5	1.5	322.7 ± 8.1	322.6 ± 8.1
YX15-668	668	581.6	1916.0	427.9	1.5	315.0 ± 5.9	315.0 ± 5.9

\*Errors are  $2\sigma$  analytical errors. Decay constant values are  $\lambda_{230} = 9.1577 \times 10^{-6} \text{ a}^{-1}$ ,  $\lambda_{234} = 2.8263 \times 10^{-6} \text{ a}^{-1}$ ,  $\lambda_{238} = 1.55125 \times 10^{-10} \text{ a}^{-1}$ . Corrected  $^{230}\text{Th}$  ages assume an initial  $^{230}\text{Th}/^{232}\text{Th}$  atomic ratio of  $(4.4 \pm 2.2) \times 10^{-6}$ . Data marked with '\*' were dated by MC-ICP-MS, whereas the other samples were measured by ICP-MS. BP here stands for 'before present' where the 'present' is defined as the year 1950 AD

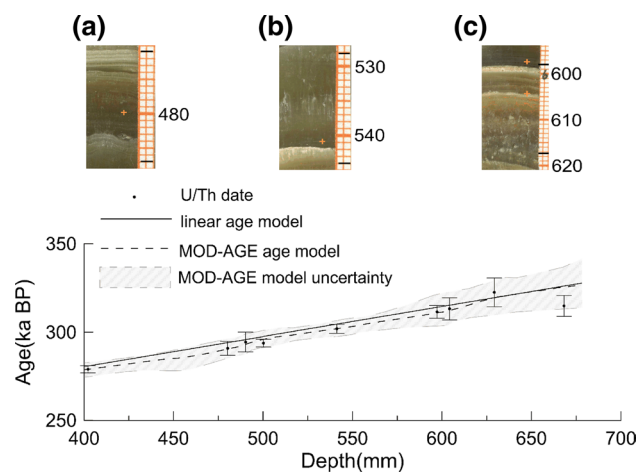


**Fig. 3** Enlarged scans and comparison of age models. **a–c** The scans are enlarged sections of abrupt shifts, with stubs marking the start and end depths of the shifts and the crosses showing the  $^{230}\text{Th}$  dating samples. The linearly interpolated age model is shown by the black line. Error bars indicate  $^{230}\text{Th}$  ages and  $2\sigma$  errors. The modelled age and the 95% confidence level are dashed and hatched, respectively

Three large amplitude  $\delta^{18}\text{O}$  shifts cover depth intervals from 617 to 598 mm, 544 to 528 mm and 487 to 471 mm (Fig. 2a). Despite an alternation of dark compact and white-porous calcite in the lowest transition, the corrected  $^{230}\text{Th}$  ages (YX15-597 and YX15-604) (Table 1 and Fig. 3c) are approximate within errors. The laminae at depths from 544 to 528 mm are transparent and dark, with one light band interlayered at a depth of 542 mm (Fig. 3b). Despite the distinct jumps in  $\delta^{18}\text{O}$  and grey-level records (Fig. 2a, c),  $\delta^{13}\text{C}$  curve decreases slowly (Fig. 2b), implying continuous deposition. The upper transition (between 487 and 471 mm) consists of transparent and dark compact calcite, gradating into translucent beige-porous laminae on the top of this section (Fig. 3a). Overall, growth of stalagmite YX15 is likely

continuous, and the abrupt signals observed in the multiproxy records probably reflect environmental changes rather than growth stops.

The chronology of stalagmite YX15 is then reconstructed based on linear interpolation due to its steady growth rate (average of  $4.7 \text{ mm ka}^{-1}$ ), except one inversion (YX15-668). To assess the linear age model, a depth age relationship was modelled using MOD-AGE, which includes a Monte Carlo simulation and allows to determine confidence intervals (Hercman and Pawlak 2012). The linear age model shows a good agreement with the MOD-AGE chronology, within  $2\sigma$  errors (Fig. 3).

### Isotopic equilibrium test

Isotopic equilibrium is a prerequisite for applying calcite isotopic data to palaeoclimate reconstructions. A strong correlation is notable in the  $\delta^{18}\text{O}$  and  $\delta^{13}\text{C}$  values along the growth axis ( $r = 0.5$ ,  $n = 279$ ), suggesting either kinetic fractionation (e.g. strong  $\text{CO}_2$  degassing and/or evaporation) (Mickler et al. 2006) or common drivers (e.g. rainfall and/or soil process) (Denniston et al. 2013). We performed Hendy tests based on twenty-five stable isotope measurements of five individual laminae (Hendy 1971). The ranges of both  $\delta^{18}\text{O}$  and  $\delta^{13}\text{C}$  values (Fig. 4a, b) within a radius of 10 mm from the growth axis (indicated by 0 mm) to the edge are small (0.6 and 0.7‰, respectively). Between adjacent points near axis (within 5 mm), differences are only 0.0 to 0.2‰ for  $\delta^{18}\text{O}$  and 0.0 to 0.3‰ for  $\delta^{13}\text{C}$ . And the ranges of  $\delta^{18}\text{O}$  and  $\delta^{13}\text{C}$  variations are equal to or smaller than those on individual horizons from the nearby Furong Cave (0.2 and 0.7‰, respectively) (Li et al. 2011), whose stalagmite precipitation has proven equilibrium. We applied a replication test (Fig. 5a, c) to further assess the robustness of the stable isotope signals (Dorale and Liu 2009). Visual inspection shows that the correspondence of LZ15  $\delta^{18}\text{O}$  record and

**Fig. 4** Results of Hendy tests. **a**  $\delta^{18}\text{O}$  and **b**  $\delta^{13}\text{C}$  variations along five individual growth layers. The results suggest that the speleothem likely deposited under equilibrium conditions

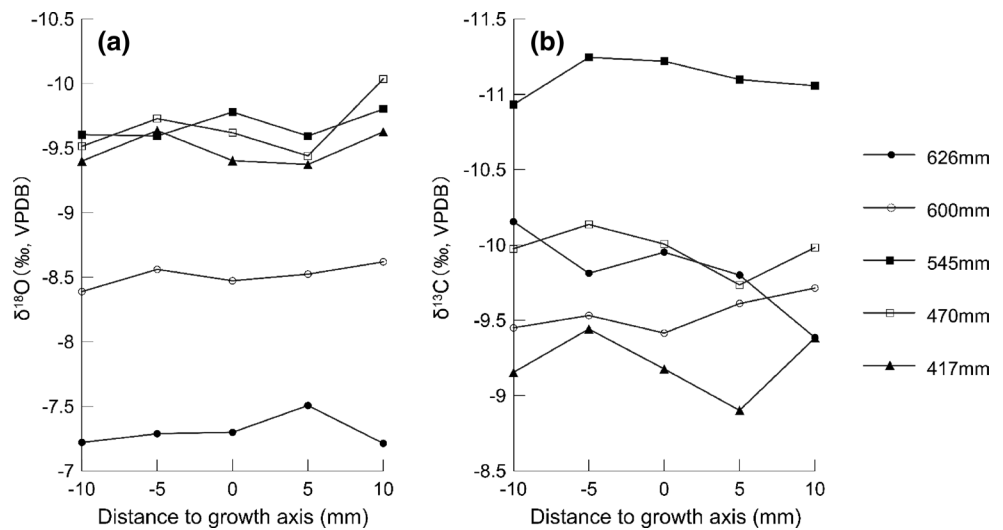
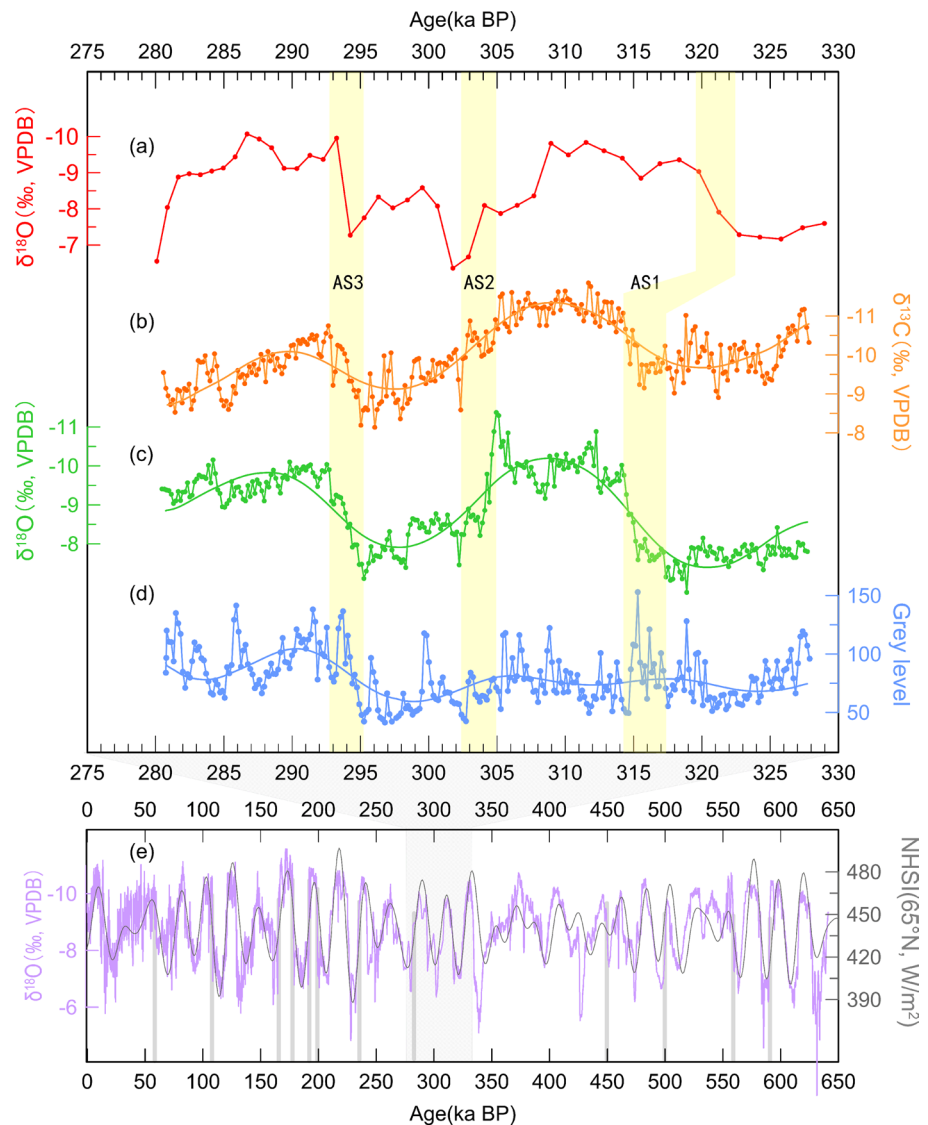


**Fig. 5** Comparison of LZ15-SB61 and YX15 records during the antepenultimate glacial period and abrupt shifts in the composite  $\delta^{18}\text{O}$  records over the past 641 ka BP. **a**  $\delta^{18}\text{O}$  record from Linzhu Cave (Cheng et al. 2009), **b** YX15  $\delta^{13}\text{C}$ , **c**  $\delta^{18}\text{O}$  and **d** grey-level records (this study), and thick smooth curves are orbital trends after removing the suborbital oscillations using change-point analysis (Taylor 2000). In order to compare the stable isotope data and the grey-level values by the same resolution, the grey-level values presented here were processed with equidistant interpolation method. **e** Composite  $\delta^{18}\text{O}$  record over the past 641 ka BP (Cheng et al. 2016) and 21 July insolation at 65°N (Berger 1978). Error bars indicate  $^{230}\text{Th}$  ages and  $2\sigma$  errors. Three bars in the upper panel depict abrupt shifts observed in the YX15  $\delta^{18}\text{O}$  record. Twelve bars in the lower panel indicate abrupt shifts



YX15  $\delta^{18}\text{O}$  record is compelling during their overlapping periods, thus indicating a climate origin for  $\delta^{18}\text{O}$  values. Therefore, we attribute the positive correlation between stable isotopic values of sample YX15 to common drivers, which are related to climate and environment. This explanation is also supported by other studies (Fairchild et al. 2006; Dorale and Liu 2009; Denniston et al. 2013).

Speleothem  $\delta^{18}\text{O}$  records from East Asia engender considerable debates and multiple interpretations with respect to the moisture source and pathways, the Indian monsoon precipitation, the hydrological process or circulation regime (Clemens et al. 2010; Dayem et al. 2010; Maher and Thompson 2012; Caley et al. 2014). However, the interpretation of the Asian Summer Monsoon (ASM) intensity on a large timescale is widely accepted (Wang et al. 2001, 2008; Cheng et al. 2009, 2016). Insofar as the modern relationship between  $\delta^{18}\text{O}$  values and monthly precipitation amounts can be applied to the past (Cobb et al. 2007; Duan et al. 2016), the minimum  $\delta^{18}\text{O}$  values can be related to stronger ASM. Recently, Liu et al. (2014) confirmed the interpretation of ASM intensity using climate models. In addition, the simulation by Caley et al. (2014) proved that calcite  $\delta^{18}\text{O}$  could be a valid ASM proxy on orbital timescales. We therefore propose the YX15  $\delta^{18}\text{O}$  as a proxy of ASM intensity, whose shifts are recorded by changes in the  $\delta^{18}\text{O}$  values of regional precipitation, at least on millennial to orbital timescales.

### Stable isotope sequences

YX15  $\delta^{18}\text{O}$  shows an amplitude of 4.6‰ (−6.8 to −11.4‰) and a mean of −9.2‰ (Fig. 5c). The  $\delta^{18}\text{O}$  profile depicts two 23-ka cycles during an interval of 47,000 years, consistent with the pattern of changing summer insolation over two precessional cycles at 65°N (Berger 1978). The broad-scale evolution of the  $\delta^{18}\text{O}$  values is divided into four distinct stages that correspond to four petrographic segments. During the first stage (327.7–314.1 ka BP), the  $\delta^{18}\text{O}$  values persist at a high level of −7.7‰ during the time interval from 327.7 to 315.3 ka BP, with one short positive period of 1500 years (318.9–317.4 ka BP) that stands out in the record. Rapid  $^{18}\text{O}$  depletion terminates this short interval, and the bulk of this shift (~2.4‰) is completed in ~1200 years (315.3–314.1 ka BP). The generally low values of  $\delta^{18}\text{O}$  in the second stage (314.1–302.2 ka BP) are characterized by two abrupt negative excursions (~1.3‰). A rapid  $^{18}\text{O}$  enrichment (from −11.4 to −7.5‰) of ~2700 years (304.9–302.2 ka BP) marks the end of the second excursion. The third stage (302.2–292.5 ka BP) is punctuated by two Weak Monsoon Intervals (WMIs), with a mean value of −8.3‰. The  $\delta^{18}\text{O}$  values then decrease rapidly from −7.1 to −10.0‰ until 292.5 ka BP, leading to the fourth phase that averages −9.5‰.

The  $\delta^{13}\text{C}$  values range between −8.1 and −11.8‰, with an average of −10.0‰ (Fig. 5b). The long-term trend in  $\delta^{13}\text{C}$  shows four intervals, analogous to the  $\delta^{18}\text{O}$  pattern. Three transitions (315.3–314.1, 304.9–302.2 and 294.9–292.5 ka BP, respectively) between the high and low levels of the  $\delta^{13}\text{C}$  values are synchronous with those displayed in the  $\delta^{18}\text{O}$  sequence (Fig. 5b, c). The following discrepancies, however, have been identified. First, the overall mean of the second phase (314.1–302.2 ka BP) (−10.9‰) in the  $\delta^{13}\text{C}$  curve is lower than that of the fourth phase (292.5–280.5 ka BP) (−9.6‰), whereas the averages of the  $\delta^{18}\text{O}$  values are similar. Second, unlike the plateau in the  $\delta^{18}\text{O}$  record, a  $^{13}\text{C}$  enrichment of ~1.9‰ covers a period from 327.4 to 324.5 ka BP. Third, the  $\delta^{13}\text{C}$  values tend to become higher along the sequence towards 280.5 ka BP, whereas the  $\delta^{18}\text{O}$  values fluctuate around a baseline with no obvious trend. Moreover, the increase in  $\delta^{13}\text{C}$  values from 292.5 to 280.5 ka BP is more distinct than in  $\delta^{18}\text{O}$ .

Therefore, the YX15 multi-proxy record, which has an average resolution of ~170 years, higher than the  $\delta^{18}\text{O}$  record from Linzhu Cave (Cheng et al. 2016), can be used as a new reference for evaluating millennial- to orbital-scale ASM changes during MIS 9.

## Discussion

### Evaluation of multiple palaeoclimate proxies

The grey level represents the albedo of the polished surface and proportion of impurities, with higher grey level corresponding to more impurities (Duan et al. 2015). Segments 2 and 4 contain abundant white impurities, and segments 1 and 3 contain minor detritus (Fig. 2d). In addition, the beige-porous laminae and white fibrous crystals correspond to lower  $\delta^{18}\text{O}$  values and the dark compact calcite to higher  $\delta^{18}\text{O}$  values (Fig. 2a, d), indicating a correlation between monsoon intensity and detrital content of the speleothem (Yadava et al. 2004; Duan et al. 2015). Similar petrographic characters were presented by Bar-Matthews et al. (1997). They hypothesized that a colder and drier climate led to a decrease in evaporation and permitted slow but continuous dripping water, and the speleothem thus incorporated little detritus. Larger amounts of impurities in speleothem formed in a warmer and wetter climate. This interpretation is applicable to the petrographic features observed in stalagmite YX15.

Most carbon in the stalagmite is derived from soil  $\text{CO}_2$ , and the soil  $\text{CO}_2$   $\delta^{13}\text{C}$  values reflect the relative abundance of  $\text{C}_4$  and  $\text{C}_3$  vegetation (Dorale et al. 1998) or the soil  $\text{CO}_2$  production (Genty et al. 2001, 2003). Considering the following aspects, we imply that YX15  $\delta^{13}\text{C}$  values reflect the degree of soil  $\text{CO}_2$  production. First, a change in the

vegetation composition cannot be invoked here, as vegetation on Mt. Shennongjia was mainly comprised of  $C_3$  plants during the last glacial and Holocene (Li et al. 2013). In addition, a drastic vegetation change in response to climate change most likely occurs during glacial–interglacial transitions (Kong et al. 2005). Second, the covariation of the stable isotopic records on orbital timescales (Fig. 5b, c) and the warm climate suggest that monsoon precipitation is the key agent controlling speleothem carbon isotope composition during MIS 9. It has been suggested that the regional hydrological cycle influences speleothem  $\delta^{13}C$  values over centennial to millennial timescales (Jo et al. 2011; Denniston et al. 2013). Such effects are introduced by changes in the soil  $CO_2$  efflux, which are affected by vegetation growth, biomass amount, microbial decomposition, root respiration and associated climate conditions (Genty et al. 2001, 2003; Grünzweig et al. 2009; Lambert and Aharon 2011; Plestenjak et al. 2012). A humid climate promotes biogenic soil activity and enhances soil  $CO_2$  production, leading to an enrichment in speleothem  $^{13}C$  (Plestenjak et al. 2012). The time lag between the monsoon intensifying and the resumption of vegetation is short for the two abrupt monsoonal strengthening, as suggested by the rapid  $\delta^{18}O$  changes and the synchronicity between  $\delta^{18}O$  and  $\delta^{13}C$  records (Fig. 5b, c). This could be explained by good soil preservation during arid periods that permits a fast onset of re-vegetation (Genty et al. 2003). Third, comparison between the  $\delta^{13}C$  and grey level shows a good correlation (Fig. 5b, d), with negative  $\delta^{13}C$  excursions corresponding to high grey-level values and vice versa. The duplication between  $\delta^{13}C$  and grey-level records likely results from the fact that more detritus absorbs and encloses higher amounts and hence enhances the stability of soil organic matters (Zech et al. 1997). A change towards rainy climate conditions leads to an increase in the amount of water percolating from the surface. There are some discrepancies between the  $\delta^{13}C$  and grey-level curves, possibly due to the different analysis tracks. The resemblance of the speleothem morphology and the stable isotopes indicates that the local karst process is responsive to regional hydrological cycle.

### Phenomena and Mechanisms of Abrupt Monsoon Shifts

As noted above, the three largest amplitude  $\delta^{18}O$  shifts greater than 2.8‰ mark the end of three stages, and they are abrupt with respect to the solar insolation changes over precession cycles (Fig. 5c). These distinct abrupt shifts are named AS1, AS2 and AS3 and are of two types: monsoon strengthening and monsoon weakening. Considering the dating errors of the interpolation and the MOD-AGE model, we estimate the age uncertainties for the midpoint of these abrupt transitions centred at  $316.0 \pm 7.8$ ,  $303.6 \pm 3.8$  and

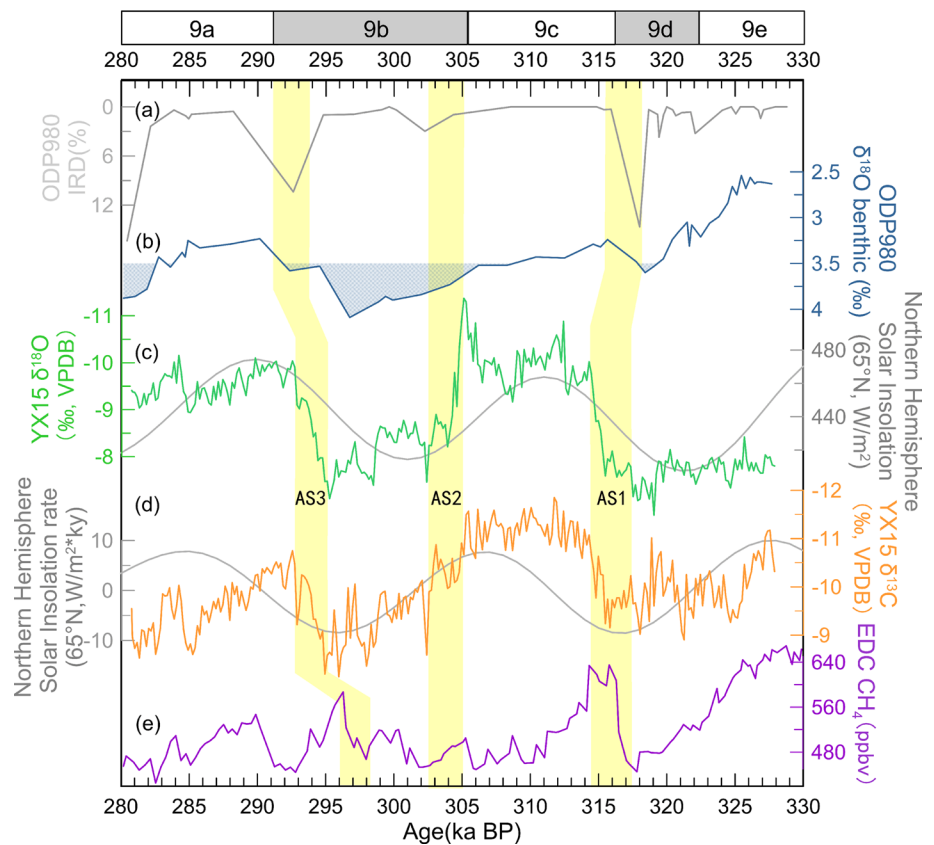
$293.9 \pm 5.0$  ka BP, respectively. These shifts are also well recognized and match the rises and drops in the LZ15  $\delta^{18}O$  record (Fig. 5a). The intensification of the ASM proceeds from WMIs centred at  $318.6 \pm 8.8$  and  $295.3 \pm 5.6$  ka BP, analogous to the pattern observed during monsoon terminations (Cheng et al. 2009, 2016). The monsoon strengthening that leads to a negative  $\delta^{18}O$  excursion of approximately  $-1.5\text{‰}$  before AS2 is consistent with a predicted Greenland warming event (Barker et al. 2011) within dating errors. And this reveals a similarity with the Chinese Interstadials A24 and A25 in the Sanbao  $\delta^{18}O$  profile (Wang et al. 2008).

Abrupt and distinct precessional shifts akin to the ASs in this study have been widely observed in late Quaternary AM records (Cheng et al. 2016). Over the past 641 ka BP (Fig. 5e), monsoonal shifts centred at approximately 558.6, 450.0, 198.8, 178.4, 106.7 and 59.6 ka BP occur on the rising limb of solar insolation, and shifts centred at approximately 590.4, 500.0, 280.6, 232.7, 191.6 and 165.8 ka BP are on the falling limb. On the contrary, some of the monsoonal shifts are concomitant in speed with insolation changes, such as the shifts centred at approximately 327.4 and 152.3 ka BP, probably due to different combinations of climate boundary conditions. These observations imply that the abruptness of monsoonal shifts is not unique character held by terminations but common over precessional cycles.

A comparison between the calcite  $\delta^{18}O$  and atmospheric  $CH_4$  records (Loulergue et al. 2008) shows a striking synchronicity around AS1 and AS3 (Fig. 6c, e), with the WMIs corresponding to minima in  $CH_4$  and the monsoon strengthening to  $CH_4$  overshoots. A similar relationship occurs around AS2; the monsoonal weakening is synchronous with  $CH_4$  decrease, respectively. In addition, the  $\delta^{13}C$  of YX15, a proxy of local soil productivity (Fig. 6d), further lends support to the link between moisture availability and low-latitude wetland expansion (Chappellaz et al. 1993). Although the ASM is strong in the long intervals after intensification,  $CH_4$  concentration peaks and then steadily decreases. These observations indicate that the boreal monsoon exerts subtle changes in  $CH_4$  emission strength. In addition, the out-of-phase relationship between  $CH_4$  and AM after abrupt intensification implies that  $CH_4$  is also modulated by north boreal high-latitude wetlands (Lehner and Döll 2004) and Southern Hemisphere tropics (Singarayer et al. 2011).

The response of land surface conditions to the low-latitude hydrology is reflected by abrupt vegetation changes. During the overlapping period, the rapid monsoonal shifts agree well with the pollen-based fast Greek vegetation evolution within dating uncertainties (Fletcher et al. 2013). Regional signals, the forest response to rapid low-latitude climate changes, are well displayed. The vegetation evolution further contributes to global  $\delta^{18}O_{atm}$  via photosynthesis (Dreyfus et al. 2007), highlighting the impact of monsoon activity on the low-latitude vegetation (Shackleton 2000).

**Fig. 6** Comparison between different records. **a** IRD and **b** benthic  $\delta^{18}\text{O}$  records from ODP980 (McManus et al. 1999). **c** YX15  $\delta^{18}\text{O}$  record and 21 July insolation at  $65^\circ\text{N}$  (Berger 1978). **d** YX15  $\delta^{13}\text{C}$  record and the insolation changing rate (Berger 1978). **e**  $\text{CH}_4$  record (Loulergue et al. 2008) on the EDC3 chronology (Parrenin et al. 2007). Three bars depict abrupt shifts



These comparisons reflect a high degree of climate coherence of widespread regions during the investigated interval and favour the idea that climate systems are tightly coupled through biosphere–atmosphere processes.

Changes in insolation control the strength of monsoon over orbital timescales (Kutzbach 1981). When boreal summer insolation rises, the ASM circulation intensifies and vice versa. A similar response is found in the YX15  $\delta^{18}\text{O}$  record, which demonstrates the strong parallelism of the minimum  $\delta^{18}\text{O}$  values with the peak summer insolation at  $65^\circ\text{N}$  (Berger 1978) (Fig. 6c). However, the end of each monsoon interval is abrupt and deviates from the gradual solar insolation changes. The amount and rate of insolation changes might be important controls on the ASs. Both shifts, AS1 and AS3, occur when the amount of insolation (Fig. 6c), along with the maximal rate in insolation rise (Fig. 6d), is average or above average. And the average here is  $440 \text{ w/m}^2$  according to the solar insolation values during the studied period. In addition, AS2 occurs when the insolation falls below this average value (Fig. 6c), consistent with the maximal rate in insolation falls as well (Fig. 6d). Each AS is completed before the insolation reaches its maximum or minimum, and this is further supported by the relationship between insolation indexes and the ASM over the last six glacial cycles. In addition, perhaps due to the forcing of insolation, the amplitudes of the ASs are magnified  $\sim 1.5$

times compared to millennial-scale events in MIS 3 (Wang et al. 2001). We assume that a threshold level of insolation exists, above or below which the monsoon response is too weak to be recorded by geological archives, and this impact probably results from the northernmost or southernmost boundaries of the ITCZ.

However, abrupt monsoonal shifts do not always occur when the magnitude and rate of solar insolation reach thresholds (e.g. the transitions at 327.4 and 152.3 ka BP). In addition, the shifts to opposite monsoon conditions apparently occur within much shorter periods, indicating a pattern that cannot be explained by gradual astronomical forcing alone (Cheng et al. 2009). The  $\delta^{18}\text{O}$  record of YX15 shows that the WMIs prior to AS1 and AS3 can be correlated with two ice-rafted debris (IRD) events and the dramatic monsoon weakening of AS2 is related to a third IRD event (Fig. 6a). We interpret these monsoon failures as times when the monsoon responds to cold anomalies generated by ice sheet disintegration and the resultant melt water that disturb the AMOC intensity at times of medium-sized ice sheets (Fig. 6b) (McManus et al. 1999). The occurrence of monsoon failures supports that the most unstable periods of glacial periods correspond to times of medium- to large-sized ice sheets (McManus et al. 1999; Siddall et al. 2010). The observation that the twelve abrupt shifts in Fig. 5e are contemporaneous with the existence of IRD layers in marine



records (McManus et al. 1999; Channell et al. 2012) supports this idea, indicating that all of the shifts occur at times when icebergs disintegrate. For example, an AS occurs at 59.6 ka BP, equivalent to the midterm of H6 within dating errors (Liu et al. 2010), and the WMI prior to Termination II synchronizes to H11 (Kelly et al. 2006).

Two types of ASs are observed, monsoon strengthening and monsoon weakening, but the mechanisms are somewhat similar, highlighting the role of ice sheets and solar insolation. The most plausible mediator that transmits the climate signals to the monsoon system is the ITCZ. On millennial timescales, it is suggested that the ITCZ responds to North Atlantic cold events (Chiang et al. 2014). Thus, for monsoonal weakening on the falling limb of the solar insolation, the WMI is boosted and develops into an AS2-type shift. Once the depression on the ITCZ via atmospheric teleconnection is removed due to the recovery of the AMOC, the ITCZ migrates northward rapidly, intensifying the monsoon. This is the case when an AS occurs on the rising limb of the insolation, with the rate of insolation changes further accelerating the monsoon transition. In addition, the ITCZ and associated monsoon are fed with abundant pre-stored latent heat and moisture derived from the Indo-Pacific Warm Pool and Indian Ocean, which are the dominant moisture sources of the ASM (Lewis et al. 2010). The moisture sources could have possibly been intercepted and reserved by the stagnated great ocean conveyor during the ‘off’ AMOC mode. Furthermore, sample YX15 documents that the abrupt monsoon intensification is accompanied by negative  $\delta^{13}\text{C}$  shifts (Fig. 6d), indicating a threshold response of soil properties and/or land cover, because land cover has the ability to modulate the monsoon intensity through soil moisture–rainfall feedbacks (Douville et al. 2001; Wei et al. 2016) and biosphere–atmosphere feedbacks (Miller et al. 2005).

## Conclusions

Stalagmite YX15 provides a centennially resolved ASM record that spans an interval from 327.7 to 280.5 ka BP. Four intervals in the  $\delta^{18}\text{O}$  and  $\delta^{13}\text{C}$  records with distinct petrography grey-level values indicate that external environmental conditions could imprint on the isotopic concentrations, organic matter and petrography of the speleothem. The stalagmite-based  $\delta^{18}\text{O}$  profile broadly follows the orbitally induced solar insolation at 65°N. The  $\delta^{13}\text{C}$  variations are essentially similar to the  $\delta^{18}\text{O}$  fluctuations in concert with two strong 23-ka cycles, indicating the sensitive response of the calcite carbon composition to climate-associated soil production on orbital timescales.

Three abrupt  $\delta^{18}\text{O}$  shifts with magnitudes greater than 2.8‰ occur during precessional transitions, similarly consistent with shifts in  $\delta^{13}\text{C}$ , grey level and petrography.

These abrupt shifts are also observed in the  $\delta^{18}\text{O}$  record from Linzhu Cave. The abrupt monsoonal shifts centred at  $316.0 \pm 7.8$ ,  $303.6 \pm 3.8$  and  $293.9 \pm 5.0$  ka BP are consistent with excursions in atmospheric  $\text{CH}_4$  and the expansion and degradation of vegetation within dating uncertainties. The WMIs and AS2 are synchronous with IRD events, further supporting a strong coupling between the northern high-latitude climate and the monsoonal system. Similar abrupt shifts are observed in the AM history over the past 641 ka BP. We suggest that an interaction between the precession-controlled insolation and the boreal ice sheet instability could be the causal agents for the abrupt ASM fluctuations on precession cycles. The ASs are initiated by the south–north shifts of the ITCZ associated with the AMOC and further amplified by soil properties and/or land cover. These precessional monsoon shifts are also modified by the solar insolation changes. Palaeoclimate reconstructions with better dating and higher resolutions as well as coupled climate models are needed to test the assumption of abrupt monsoonal shifts on precession cycles.

**Acknowledgements** The authors are grateful to the Editor-in-Chief Dr. Dörhöfer and the two anonymous reviewers for their constructive comments which significantly improved the manuscript. This work was supported by grants of National Nature Science Foundation of China (41130210, 41072126 and 41572340), Priority Academic Program Development of Jiangsu Higher Education Institutions, National Key Basic Research Program of China (2015CB953804) and US Nature Science Foundation (1103403).

## References

- Barker S, Knorr G, Edwards RL, Parrenin F, Putnam AE, Skinner LC, Wolff E, Ziegler M (2011) 800,000 years of abrupt climate variability. *Science* 334:347–351
- Bar-Matthews M, Ayalon A, Kaufman A (1997) Late Quaternary paleoclimate in the eastern Mediterranean region from stable isotope analysis of speleothems at Soreq Cave, Israel. *Quat Res* 47:155–168
- Berger AL (1978) Long-term variations of caloric insolation resulting from the Earth’s orbital elements. *Quat Res* 9:139–167
- Caley T, Roche DM, Renssen H (2014) Orbital Asian summer monsoon dynamics revealed using an isotope-enabled global climate model. *Nat Commun* 5:5371. <https://doi.org/10.1038/ncomms6371>
- Channell JET, Hodell DA, Romero O, Hillaire-Marcel C, de Vernal A, Stoner JS, Mazaud A, Röhl U (2012) A 750-kyr detrital-layer stratigraphy for the North Atlantic (IODP Sites U1302–U1303, Orphan Knoll, Labrador Sea). *Earth Planet Sci Lett* 317–318:218–230
- Chappellaz J, Blunier T, Raynaud D, Barnola JM, Schwander J, Stauffer B (1993) Synchronous changes in atmospheric  $\text{CH}_4$  and Greenland climate between 40 and 8 kyr BP. *Nature* 366:443–445
- Cheng H, Edwards RL, Broecker WS, Denton GH, Kong XG, Wang YJ, Zhang R, Wang XF (2009) Ice age terminations. *Science* 326:248–252
- Cheng H, Edwards RL, Shen CC, Polyak VJ, Asmerom Y, Woodhead J, Hellstrom J, Wang YJ, Kong XG, Spötl C, Wang XF, Calvin Alexander E Jr (2013) Improvements in  $^{230}\text{Th}$  dating,  $^{230}\text{Th}$  and

- $^{234}\text{U}$  half-life values, and U-Th isotopic measurements by multi-collector inductively coupled plasma mass spectrometry. *Earth Planet Sci Lett* 371–372:82–91
- Cheng H, Edwards RL, Sinha A, Spötl C, Yi L, Chen ST, Kelly M, Kathayat G, Wang XF, Li XL, Kong XG, Wang YJ, Ning YF, Zhang HW (2016) The Asian monsoon over the past 640,000 years and ice age terminations. *Nature* 534:640–646
- Chiang JCH, Lee SY, Putnam AE, Wang XF (2014) South Pacific Split Jet, ITCZ shifts, and atmospheric North-South linkages during abrupt climate changes of the last glacial period. *Earth Planet Sci Lett* 406:233–246
- Clemens SC, Prell WL, Sun YB (2010) Orbital-scale timing and mechanisms driving Late Pleistocene Indo-Asian summer monsoons: reinterpreting cave speleothem  $\delta^{18}\text{O}$ . *Paleoceanography* 25:PA4207. <https://doi.org/10.1029/2010pa001926>
- Cobb KM, Adkins JF, Partin JW, Clark B (2007) Regional-scale climate influences on temporal variations of rainwater and cave dripwater oxygen isotopes in northern Borneo. *Earth Planet Sci Lett* 263:207–220
- Dayem KE, Molnar P, Battisti DS, Roe GH (2010) Lessons learned from oxygen isotopes in modern precipitation applied to interpretation of speleothem records of paleoclimate from eastern Asia. *Earth Planet Sci Lett* 295:219–230
- deMenocal P, Ortiz J, Guilderson T, Adkins J, Sarnthein M, Baker L, Yarusinsky M (2000) Abrupt onset and termination of the African Humid Period: rapid climate responses to gradual insolation forcing. *Quat Sci Rev* 19:347–361
- Denniston RF, Asmerom Y, Lachniet M, Polyak VJ, Hope P, An N, Rodzinyak K, Humphreys WF (2013) A Last Glacial Maximum through middle Holocene stalagmite record of coastal Western Australia climate. *Quat Sci Rev* 77:101–112
- Dorale JA, Liu ZH (2009) Limitations of Hendy test criteria in judging the paleoclimatic suitability of speleothems and the need for replication. *J Cave Karst Stud* 71:73–80
- Dorale JA, Edwards RL, Ito E, González LA (1998) Climate and vegetation history of the midcontinent from 75 to 25 ka: a speleothem record from Crevice Cave, Missouri, USA. *Science* 282:1871–1874
- Douville H, Chauvin F, Broqua H (2001) Influence of soil moisture on the Asian and African monsoons. Part I: mean monsoon and daily precipitation. *J Clim* 14:2381–2403
- Dreyfus GB, Parrenin F, Lemieux-Dudon B, Durand G, Masson-Delmotte V, Jouzel J, Barnola JM, Panno L, Spahni R, Tisserand A, Siegenthaler U, Leuenberger M (2007) Anomalous flow below 2700 m in the EPICA Dome C ice core detected using  $\delta^{18}\text{O}$  of atmospheric oxygen measurements. *Clim Past* 3:341–353
- Duan FC, Wu JY, Wang YJ, Edwards RL, Cheng H, Kong XG, Zhang WH (2015) A 3000-yr annually laminated stalagmite record of the Last Glacial Maximum from Hulu Cave, China. *Quat Res* 83:360–369
- Duan WH, Ruan JY, Luo WJ, Li TY, Tian LJ, Zeng GN, Zhang DZ, Naid YJ, Li JL, Tao T, Zhang PZ, Baker A, Tan M (2016) The transfer of seasonal isotopic variability between precipitation and drip water at eight caves in the monsoon regions of China. *Geochim Cosmochim Acta* 183:250–266
- Fairchild IJ, Smith CL, Baker A, Fuller L, Spötl C, Matthey D, McDermott F (2006) Modification and preservation of environmental signals in speleothems. *Earth Sci Rev* 75:105–153
- Fletcher WJ, Müller UC, Koutsodendris A, Christanis K, Pross J (2013) A centennial-scale record of vegetation and climate variability from 312 to 240 ka (Marine Isotope Stages 9c-a, 8 and 7e) from Tenaha Philippon, NE Greece. *Quat Sci Rev* 78:108–125
- Genty D, Baker A, Massault M, Proctor C, Gilmour M, Pons-Branchu E, Hamelin B (2001) Dead carbon in stalagmites: carbonate bedrock paleodissolution vs. ageing of soil organic matter. Implications for  $^{13}\text{C}$  variations in speleothems. *Geochim Cosmochim Acta* 65:3443–3457
- Genty D, Blamart D, Ouahdi R, Gilmour M, Baker A, Jouzel J, Van-Exter S (2003) Precise dating of Dansgaard-Oeschger climate oscillations in western Europe from stalagmite data. *Nature* 421:833–837
- Grünzweig JM, Hemming D, Maseyk K, Lin TB, Rotenberg E, Raz-Yaseef N, Falloon PD, Yakir D (2009) Water limitation to soil  $\text{CO}_2$  efflux in a pine forest at the semiarid “timberline”. *J Geophys Res* 114:G03008. <https://doi.org/10.1029/2008JG000874>
- Hendy CH (1971) The isotopic geochemistry of speleothems—I. The calculation of the effects of different modes of formation on the isotopic composition of speleothems and their applicability as palaeoclimatic indicators. *Geochim Cosmochim Acta* 3:801–824
- Hercman H, Pawlak J (2012) MOD-AGE: an age-depth model construction algorithm. *Quat Geochronol* 12:1–10
- Jo KN, Woo KS, Lim HS, Cheng H, Edwards RL, Wang YJ, Jiang XY, Kim R, Lee JI, Yoon HI, Yoo KC (2011) Holocene and Eemian climatic optima in the Korean Peninsula based on textural and carbon isotopic records from the stalagmite of the Daeya Cave, South Korea. *Quat Sci Rev* 30:1218–1231
- Kelly MJ, Edwards RL, Cheng H, Yuan DX, Cai YJ, Zhang ML, Lin YS, An ZS (2006) High resolution characterization of the Asian Monsoon between 146,000 and 99,000 years BP from Dongge Cave, China and global correlation of events surrounding Termination II. *Palaeogeogr Palaeoclimatol Palaeoecol* 236:20–38
- Kong XG, Wang YJ, Wu JY, Cheng H, Edwards RL, Wang XF (2005) Complicated responses of stalagmite  $\delta^{13}\text{C}$  to climate change during the last glaciation from Hulu Cave, Nanjing, China. *Sci China Ser D Earth Sci* 48:2174–2181
- Kutzbach JE (1981) Monsoon climate of the early Holocene: climate experiment with the earth's orbital parameters for 9,000 years ago. *Science* 214:59–61
- Lambert WJ, Aharon P (2011) Controls on dissolved inorganic carbon and  $\delta^{13}\text{C}$  in cave waters from DeSoto Caverns: implications for speleothem  $\delta^{13}\text{C}$  assessments. *Geochim Cosmochim Acta* 75:753–768
- Lehner B, Döll P (2004) Development and validation of a global database of lakes, reservoirs and wetlands. *J Hydrol* 296:1–22
- Levermann A, Schewe J, Petoukhov V, Held H (2009) Basic mechanism for abrupt monsoon transitions. *Proc Natl Acad Sci USA* 106:20572–20577
- Lewis SC, Legrande AN, Kelly M, Schmidt GA (2010) Water vapour source impacts on oxygen isotope variability in tropical precipitation during Heinrich events. *Clim Past* 6:325–343
- Li TY, Shen CC, Li HC, Li JY, Chiang HW, Song SR, Yuan DX, Lin CDJ, Gao P, Zhou LP, Wang JL, Ye MY, Tang LL, Xie SY (2011) Oxygen and carbon isotopic systematics of aragonite speleothems and water in Furong Cave, Chongqing, China. *Geochim Cosmochim Acta* 75:4140–4156
- Li J, Zheng Z, Huang KY, Yang SX, Chase B, Valsecchi V, Carré M, Cheddadi R (2013) Vegetation changes during the past 40,000 years in Central China from a long fossil record. *Quat Int* 310:221–226
- Liu DB, Wang YJ, Cheng H, Edwards RL, Kong XG, Wang XF, Hardt B, Wu JY, Chen ST, Jiang XY, He YQ, Dong JG, Zhao K (2010) Sub-millennial variability of Asian monsoon intensity during the early MIS 3 and its analogue to the ice age terminations. *Quat Sci Rev* 29:1107–1115
- Liu ZY, Wen XY, Brady EC, Otto-Bliesner B, Yu G, Lu HY, Cheng H, Wang YJ, Zheng WP, Ding YH, Edwards RL, Cheng J, Liu W, Yang H (2014) Chinese cave records and the East Asia Summer Monsoon. *Quat Sci Rev* 83:115–128
- Loulergue L, Schilt A, Spahni R, Masson-Delmotte V, Blunier T, Lemieux B, Barnola JM, Raynaud D, Stocker TF, Chappellaz J

- (2008) Orbital and millennial-scale features of atmospheric CH<sub>4</sub> over the past 800,000 years. *Nature* 453:383–386
- Maher BA, Thompson R (2012) Oxygen isotopes from Chinese caves: records not of monsoon rainfall but of circulation regime. *J Quat Sci* 27:615–624
- McManus JF, Oppo DW, Cullen JL (1999) A 0.5-million-year record of millennial-scale climate variability in the North Atlantic. *Science* 283:971–975
- Mickler PJ, Stern LA, Banner JL (2006) Large kinetic isotope effects in modern speleothems. *Geol Soc Am Bull* 118:65–81
- Miller G, Mangan J, Pollard D, Thompson S, Felzer B, Magee J (2005) Sensitivity of the Australian monsoon to insolation and vegetation: implications for human impact on continental moisture balance. *Geology* 33:65–68
- Mohtadi M, Prange M, Steinke S (2016) Palaeoclimatic insights into forcing and response of monsoon rainfall. *Nature* 533:191–199
- Parrenin F, Barnola JM, Beer J, Blunier T, Castellano E, Chappellaz J, Dreyfus G, Fischer H, Fujita S, Jouzel J, Kawamura K, Lemieux-Dudon B, Loulergue L, Masson-Delmotte V, Narcisi B, Petit JR, Raisbeck G, Raynaud D, Ruth U, Schwander J, Severi M, Spahni R, Steffensen JP, Svensson A, Udisti R, Waelbroeck C, Wolff E (2007) The EDC3 chronology for the EPICA Dome C ice core. *Clim Past* 3:485–497
- Petit JR, Jouzel J, Raynaud D, Barkov NI, Barnola JM, Basile I, Bender M, Chappellaz J, Davis M, Delaygue G, Delmotte M, Kotlyakov VM, Legrand M, Lipenkov VY, Lorius C, Pépin L, Ritz C, Saltzman E, Stievenard M (1999) Climate and atmospheric history of the past 420,000 years from the Vostok ice core, Antarctica. *Nature* 399:429–436
- Plestenjak G, Eler K, Vodnik D, Ferlan M, Čater M, Kanduč T, Simončič P, Ogrinc N (2012) Sources of soil CO<sub>2</sub> in calcareous grassland with woody plant encroachment. *J Soil Sediment* 12:1327–1338
- Schaefer JM, Putnam AE, Denton GH, Kaplan MR, Birkel S, Doughty AM, Kelley S, Barrell DJA, Finkel RC, Winckler G, Anderson RF, Ninneman US, Barker S, Schwartz R, Andersen BG, Schluechter C (2015) The southern glacial maximum 65,000 years ago and its unfinished termination. *Quat Sci Rev* 114:52–60
- Shackleton NJ (2000) The 100,000-year ice-age cycle identified and found to lag temperature, carbon dioxide, and orbital eccentricity. *Science* 289:1897–1902
- Siddall M, Rohling EJ, Blunier T, Spahni R (2010) Patterns of millennial variability over the last 500 ka. *Clim Past* 6:295–303
- Singarayer JS, Valdes PJ, Friedlingstein P, Nelson S, Beerling DJ (2011) Late Holocene methane rise caused by orbitally controlled increase in tropical sources. *Nature* 470:82–85
- Taylor WA (2000) Change-point analysis: a powerful new tool for detecting changes. Taylor Enterprises, Inc. <http://www.variation.com/cpa/tech/changepoint.html>. Accessed 8 Sep 2017
- Wang YJ, Cheng H, Edwards RL, An ZS, Wu JY, Shen CC, Dorale JA (2001) A high-resolution absolute-dated late Pleistocene monsoon record from Hulu Cave, China. *Science* 294:2345–2348
- Wang YJ, Cheng H, Edwards RL, Kong XG, Shao XH, Chen ST, Wu JY, Jiang XY, Wang XF, An ZS (2008) Millennial- and orbital-scale changes in the East Asian monsoon over the past 224,000 years. *Nature* 451:1090–1093
- Wei JF, Su H, Yang ZL (2016) Impact of moisture flux convergence and soil moisture on precipitation: a case study for the southern United States with implications for the globe. *Clim Dyn* 46:467–481
- Wolff EW, Fischer H, Röthlisberger R (2009) Glacial terminations as southern warmings without northern control. *Nat Geosci* 2:206–209
- Yadava MG, Ramesh R, Pant GB (2004) Past monsoon rainfall variations in peninsular India recorded in a 331-year-old speleothem. *Holocene* 14:517–524
- Yuan DX, Cheng H, Edwards RL, Dykoski CA, Kelly MJ, Zhang ML, Qing JM, Lin YS, Wang YJ, Wu JY, Dorale JA, An ZS, Cai YJ (2004) Timing, duration, and transitions of the last interglacial Asian monsoon. *Science* 304:575–578
- Zech W, Senesi N, Guggenberger G, Kaiser K, Lehmann J, Miano TM, Miltner A, Schroth G (1997) Factors controlling humification and mineralization of soil organic matter in the tropics. *Geoderma* 79:117–161
- Ziegler M, Tuenter E, Lourens LJ (2010) The precession phase of the boreal summer monsoon as viewed from the Eastern Mediterranean (ODP site 968). *Quat Sci Rev* 29:1481–1490